frontiers in Earth Science

ORIGINAL RESEARCH
published: 19 October 2018
doi: 10.3389/feart.2018.00166

Early Holocene Establishment of the Barents Sea Arctic Front

Bjørg Risebrobakken[1]* *and Sarah M. P. Berben*[2]

[1] NORCE Norwegian Research Centre, Bjerknes Centre for Climate Research, Bergen, Norway, [2] Department of Earth Science, University of Bergen, Bjerknes Centre for Climate Research, Bergen, Norway

A main feature of the Barents Sea oceanography is the Arctic front. The Arctic front marks the transition between the dominating water masses of the Barents Sea: Atlantic Water in the south and Arctic Water in the north. Presently, the Barents Sea Arctic front is directed by the topography of the Bear Island Trough and to some degree the location of the sea ice boundary. During the last glacial maximum, the Svalbard-Barents Sea and Scandinavian Ice Sheets covered the Barents Sea. Hence, no water entered the Barents Sea, neither from the south nor from the north. Following the deglaciation of the Barents Sea, the present-day ocean circulation developed. The evolution of how the present location of the Barents Sea Arctic front established during the early Holocene is documented by foraminiferal relative assemblage data from six core sites along the western Barents Sea margin and opening. The relative abundance of Arctic front indicator *Turborotalita quinqueloba*, in combination with the cold, polar *Neogloboquadrina pachyderma* and warm, Atlantic *Neogloboquadrina incompta*, are used to infer the location of the Barents Sea Arctic front relative to the individual core sites. Until ca. 11 ka BP, the Barents Sea Arctic front followed the western margin of the Barents Sea. All sites along the Barents Sea margin where still dominated by Arctic Water between ca. 11 and 10.2 ka BP, however, the Barents Sea Arctic front turned eastwards into the southwestern Barents Sea. From ca. 10.2 to 8.8 ka BP, the Barents Sea Arctic front moved eastward and was located right above most sites as it followed the Barents Sea margin. The northwestern Barents Sea Arctic front was close to the present location from ca. 8.8 to 7.4 ka BP, however, it was still confined to the southwestern Barents Sea. From ca. 7.4 ka BP, the Barents Sea Arctic front has been located close to the present position, along the margin southwards from Svalbard, turning eastwards along and beyond the northern Bear Island Trough margin.

Keywords: Barents Sea, Arctic front, Holocene, planktic foraminifera, oceanography, Atlantic Water, Arctic Water

OPEN ACCESS

Edited by:
Evgenia Kandiano, GEOMAR Helmholtz-Zentrum für Ozeanforschung Kiel (HZ), Germany

Reviewed by:
Robert F. Spielhagen, GEOMAR Helmholtz-Zentrum für Ozeanforschung Kiel (HZ), Germany
Anastasia Zhuravleva, Akademie der Wissenschaften und der Literatur Mainz, Germany

***Correspondence:**
Bjørg Risebrobakken
bjri@norceresearch.no

Specialty section:
This article was submitted to Quaternary Science, Geomorphology and Paleoenvironment, a section of the journal Frontiers in Earth Science

Received: *25 June 2018*
Accepted: *28 September 2018*
Published: *19 October 2018*

Citation:
Risebrobakken B and Berben SMP (2018) Early Holocene Establishment of the Barents Sea Arctic Front. Front. Earth Sci. 6:166. doi: 10.3389/feart.2018.00166

INTRODUCTION

The Barents Sea and the Fram Strait are the major pathways for Atlantic Water entering the Arctic Ocean (**Figure 1A**) (e.g., Carmack et al., 2006; Rudels et al., 2015). Furthermore, the Barents Sea is an area of extensive water mass transformation and ocean-atmosphere heat exchange (Smedsrud et al., 2013). In particular, the Norwegian Atlantic Current (NwAC) transports Atlantic Water northwards until it splits into two branches with one of them entering the Barents Sea (**Figure 1A**; Blindheim and Østerhus, 2005). More specifically, the North Cape Current (NCaC) turns into

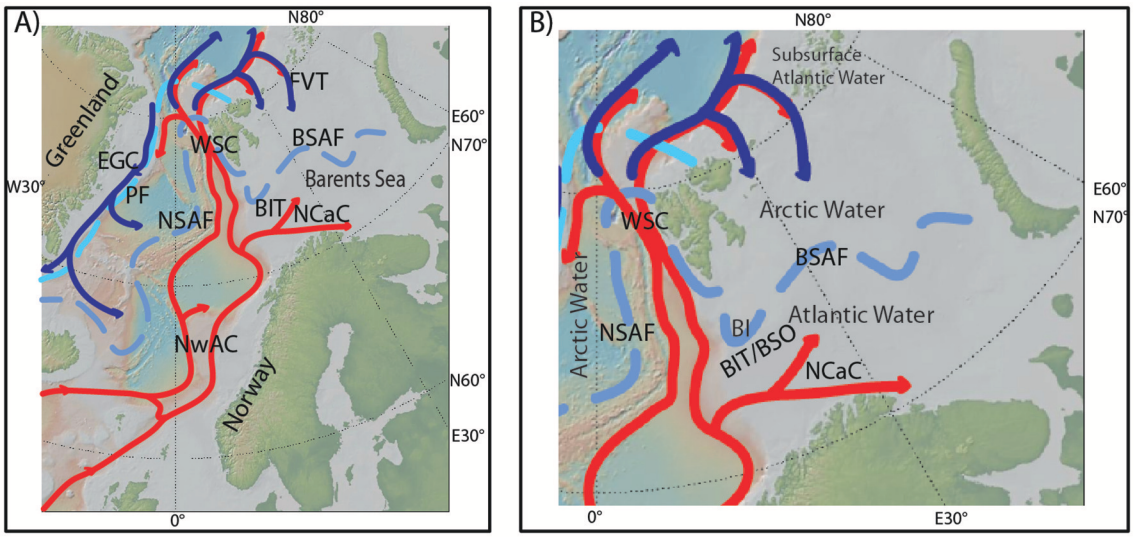

FIGURE 1 | (A) Main features of present-day surface to subsurface oceanography of the Nordic Seas and the Barents Sea. NwAC, Norwegian Atlantic Current; NCaC, North Cape Current; WSC, West Spitsbergen Current; EGC, East Greenland Current; PF, Polar front; NSAF, Nordic Seas Arctic front; BSAF, Barents Sea Arctic front; BIT, Bear Island Trough; FVT, Franz Victoria Trough. **(B)** Close-up map of the Barents Sea and the main present-day oceanographic features. Atlantic Water is found south of the BSAF, Arctic Water is found north of the BSAF. In the Northern Barents Sea, Atlantic Water is found at the subsurface, underneath the Arctic Water. BIT/BSO, Bear Island Trough/Barents Sea Opening; BI, Bear Island. Maps are created using GeoMapApp, http://geomapapp.org.

the Barents Sea through the Bear Island Trough (BIT) whereas the West Spitsbergen Current (WSC) flows northwards along the western Barents Sea margin and enters the Arctic Ocean through the Fram Strait (**Figure 1A**). Consequently, the southern Barents Sea is bathed by warm, saline Atlantic Water (**Figure 1B**; Loeng, 1991). Contrary, in the north, Polar Water flows, within the upper part of the water column, southwards from the Arctic Ocean via the Franz Victoria Trough (FVT) into the Barents Sea and forms Arctic Water when it meets and mixes with Atlantic Water (Hopkins, 1991; **Figure 1A**). Thereby, the northern Barents Sea becomes dominated with Arctic Water with lower temperatures and salinities compared to the Atlantic Water in the southern part of the Barents Sea (**Figure 1B**). Atlantic Water is only found at greater depths, below the Arctic Water, in the northern Barents Sea.

The Arctic Water in the northern and the Atlantic Water in the southern Barents Sea are separated by the Barents Sea Arctic front (BSAF), also referred to as the Polar front, a dominant oceanographic feature of the near-surface waters of the Barents Sea (Loeng, 1991; Pfirman et al., 1994; Parsons et al., 1996). The BSAF follows the western Svalbard and Barents Sea margins southwards from Svalbard and turns eastward into the interior Barents Sea south of Bear Island (**Figures 1A,B**). In the western Barents Sea, the BSAF is topographically constrained and well defined, following the northern margin of the BIT (Loeng, 1991; Parsons et al., 1996; Harris et al., 1998). Farther east, where the topographic features are less well pronounced, the BSAF is consequently less well defined and more dependent on the strength of the Atlantic Water inflow through the NCaC (Loeng, 1991; Parsons et al., 1996; Loeng and Drinkwater, 2007). The BSAF is a perennial feature, closely related to the overall sea ice conditions and, in particular, it often follows the winter sea ice margin (Vinje, 1977).

The Barents Sea experiences strong seasonal sea ice variability (Kvingedal, 2005). September is characterized by a minimum sea ice concentration, while the sea ice extent reaches its yearly maximum position in April (Sorteberg and Kvingedal, 2006). Sea ice melting during summer creates a warm, fresh summer mixed layer. Underneath the summer mixed layer a moderate temperature gradient is seen between the Atlantic and Arctic Water masses, respectively in the southern and northern parts of the Barents Sea (Parsons et al., 1996). Local ice formation takes place when the summer melt layer refreezes during the following winter (Harris et al., 1998). In addition, wind dependent sea ice transport from the Arctic Ocean may take place (Kwok et al., 2005; Sorteberg and Kvingedal, 2006; Kwok, 2009).

In stark contrast to the present-day situation, the Barents Sea was covered by the Svalbard-Barents Sea Ice Sheet merging with the Scandinavian Ice Sheet during the last glacial maximum and until ca. 16 ka BP (Hughes et al., 2016). At that time the present shallow epicontinental sea, with a mean water depth of ca. 230 m, did not exist. Hence, the Barents Sea experienced an extensive transformation from the time of total ice sheet coverage until its present oceanographic state characterized by the southern Atlantic and northern Arctic domains, separated by the BSAF. As the ice sheets retreated the ocean took over. During the deglaciation periods of cold open surface waters, winter sea ice and weak subsurface inflow of Atlantic Water as well as severe cold conditions with an extensive sea ice cover took place in the southwestern Barents Sea (Aagaard-Sørensen et al., 2010; Chistyakova et al., 2010). During the early phase of the Holocene, ca. 11 to 7.5 ka BP, winter sea ice was replaced by

a warm and fresh summer mixed layer, on top of warm bottom water (Risebrobakken et al., 2010). Seasonal sea ice and surface freshening is also documented just north of Bear Island, at the western Barents Sea margin, until ca. 10.4 ka BP, followed by a declining seasonal sea ice cover and enhanced influence of Atlantic Water until ca. 7.3 ka BP (Berben et al., 2014). Atlantic Water was, as in the southwestern Barents Sea, continuously present as bottom water (Groot et al., 2014). The northern Barents Sea was influenced by meltwater and reduced salinities until ca. 11 ka BP (Klitgaard-Kristensen et al., 2013). Enhanced influence of Atlantic Water has been argued to cause the recorded minimum in Holocene seasonal sea ice extent, between ca. 9.5 and 5.9 ka BP (Berben et al., 2017). No study has so far integrated directly comparable information from spatially spread marine sediment cores to investigate the establishment of the BSAF, the main oceanographic feature of today's Barents Sea.

Different planktic foraminiferal species have different preferences for their living habitat. These differences can be utilized to assess the location of past oceanographic characteristics. Here, we will document the establishment of the BSAF, as an expression of the approximate interface between Atlantic and Arctic Water, through the early Holocene, following the deglaciation of the Svalbard-Barents Sea and Scandinavian Ice Sheets. We will do so by (1) synthesizing planktic foraminiferal assemblage data from six marine sediment cores from the western Barents Sea margin and opening (**Figures 2A,B**) and (2) using the relative relation between the dominant species found in these sediment cores, *Turborotalita quinqueloba*, *Neogloboquadrina pachyderma* and *Neogloboquadrina incompta*, to map the location of the BSAF relative to the individual core sites and infer the location between the sites. These three species have a preference for frontal conditions, Arctic/Polar Water and Atlantic Water, respectively (Bé and Tolderlund, 1971; Johannessen et al., 1994; Pflaumann et al., 2003; Husum and Hald, 2012). Furthermore, we will discuss potential linkages between upstream changes in advection of Atlantic Water and the identified timing of the four-step development of the BSAF establishment.

MATERIALS AND METHODS

Relative abundance of planktic foraminifera from six sediment cores from the western Barents Sea margin and opening are synthesized (**Figure 2**). All records are previously published (Hald et al., 1996, 2007; Hald and Aspeli, 1997; Sarnthein et al., 2003; Ebbesen et al., 2007; Risebrobakken et al., 2010; Berben et al., 2014). The records have, however, never before been integrated and used to inform on the establishment of the BSAF after the last deglaciation. Core names, locations, water depths and references to original publications are given in **Table 1**. PSh-5159N, T-88-2, MD99-2304 and JM09-KA11-GC are counted at the size fraction $\geq$100 μm, while T-79-51/2 and M23258 were counted at $\geq$125 μm and $\geq$150 μm, respectively. Further details about the methods can be found in the original publications (Hald et al., 1996, 2007; Hald and Aspeli, 1997; Sarnthein et al., 2003; Ebbesen et al., 2007; Risebrobakken et al., 2010; Berben et al., 2014).

In this study, the age models are based on previously published age models for the cores (Hald et al., 2007; Risebrobakken et al., 2011; Berben et al., 2014). To ensure a consistent chronological frame work all ^{14}C AMS dates have, however, been recalibrated using the Marine13 radiocarbon calibration curve (Reimer et al., 2013) and a $\Delta R = 71 \pm 21$ (Mangerud et al., 2006) in Calib 7.1 (Stuiver and Reimer, 1993; **Table 2**). The main difference to previously published chronologies is caused by the fact that those used a variety of ΔR values and different versions of the radiocarbon calibration curve. Where Vedde ash was identified the age from Rasmussen et al. (2006) is used. The age models are calculated based on a linear interpolation between the tie-points defined by the median probability of the calibrated radiocarbon dates and when present, the Vedde ash layer. In T-88-2 one of eleven, and in M23258 one of fifteen, ^{14}C AMS dates are not used due to inverted ages. In core JM09-KA11-GC five of thirteen ^{14}C AMS dates are discarded due to inversions. Four of these discarded ages, two from the same core-depth, were measured on mollusc fragments and are considered less reliable than nearby dated foraminifera. For cores PSh-5159N, MD99-2304 and T-79-51/2 all existing ^{14}C AMS dates are used.

In all six cores the planktic foraminiferal fauna has been dominated by *N. pachyderma*, *N. incompta* and *T. quinqueloba*. *Neogloboquadrina pachyderma* is a cold-water species that dominates the fauna in Arctic and Polar Water masses (Bé and Tolderlund, 1971; Johannessen et al., 1994; Pflaumann et al., 2003; Husum and Hald, 2012) where it is found to constitute 96-99% of the assemblage, independent of the counted size fraction ($\geq$100 μm or $\geq$150 μm) (Husum and Hald, 2012). *Neogloboquadrina pachyderma* is, however, also the dominant species in chilled Atlantic derived water, as presently found in the Fram Strait (Pflaumann et al., 2003; Husum and Hald, 2012). *Neogloboquadrina incompta* is a warm water species that dominates the fauna associated with Atlantic Water in the Nordic Seas (Bé and Tolderlund, 1971; Johannessen et al., 1994). Relative abundances of up to 45% ($\geq$100 μm) of *N. incompta* have, however, also been observed in warm Coastal Water off northern Norway (Husum and Hald, 2012). *Turborotalita quinqueloba* is a subpolar species that dominates the fauna in Arctic areas influenced by Atlantic Water and is most frequently found in the vicinity of the Arctic front in the Nordic Seas and in the Barents Sea (Johannessen et al., 1994; Pflaumann et al., 2003; Husum and Hald, 2012). Husum and Hald (2012) found more than 50% of *T. quinqueloba* ($\geq$100 μm) close to the Arctic front in the northwestern Barents Sea, while Johannessen et al. (1994) documented up to 70% of *T. quinqueloba* ($\geq$125 μm) by the Nordic Seas Arctic front. Minor contributions of other species found in the investigated cores are all associated with warm Atlantic Water (*Globigerina bulloides; Globigerinita glutinata; Globigerinoides ruber; Globigerina falconensis*), with the exception of *Globigerinita uvula* which reaches its highest relative abundances in Coastal Water (Husum and Hald, 2012).

The distinct different water mass preferences of the three main planktic foraminifera species are used in a simple first order approach to identify the location of the BSAF following the last

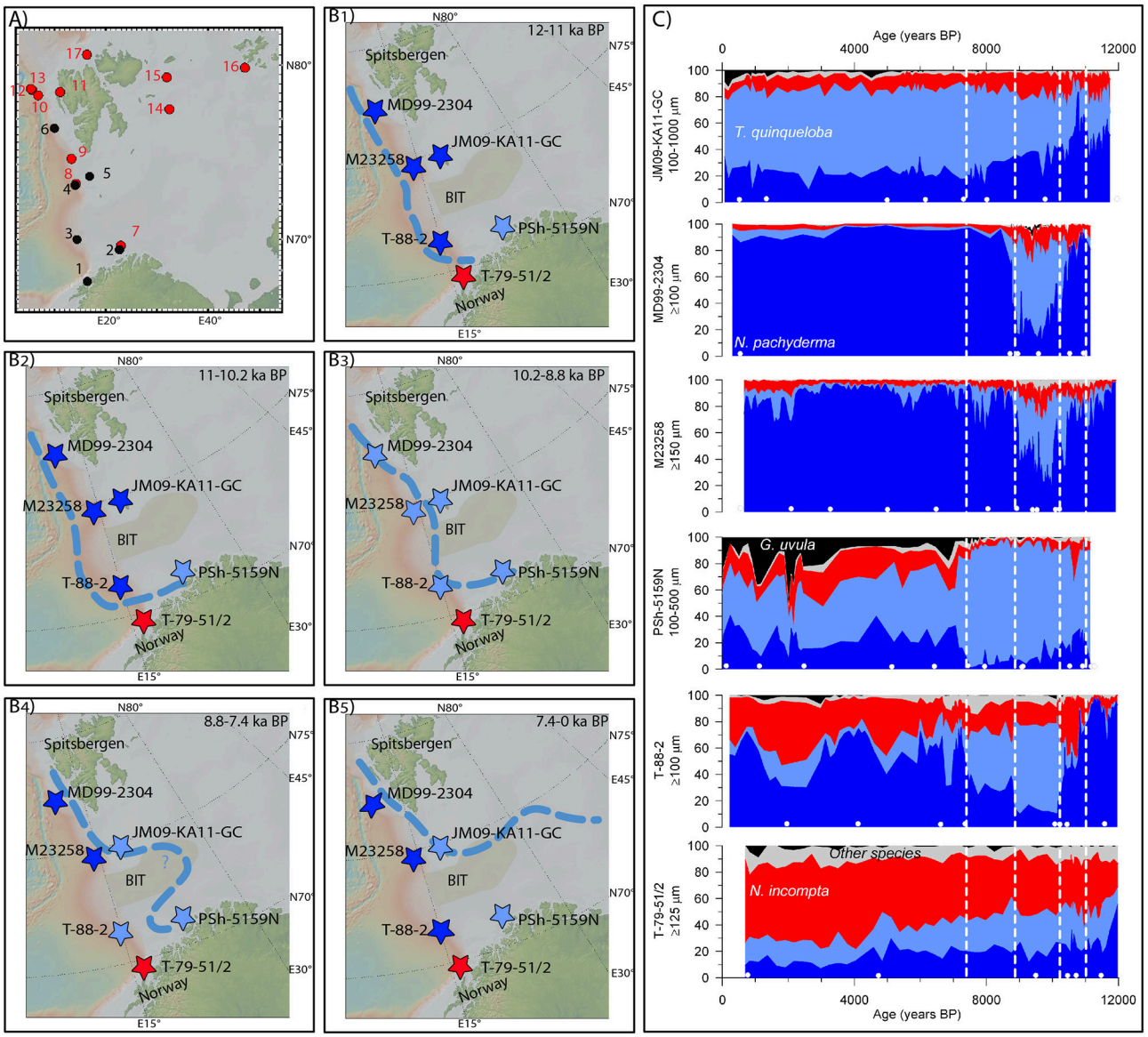

FIGURE 2 | (A) Map showing the location of the investigated cores (black) and cores from other studies mentioned in the discussion (red). (1) T-79-51/2 (Hald et al., 1996). (2) PSh-5159N (Risebrobakken et al., 2010). (3) T-88-2 (Hald and Aspeli, 1997; Hald et al., 2007). (4) M23258 (Sarnthein et al., 2003). (5) JM09-KA11-GC (Berben et al., 2014). (6) MD99-2304 (Ebbesen et al., 2007). (7) JM05-085-GC (Aagaard-Sørensen et al., 2010). (8) SV-04 (Rigual-Hernández et al., 2017). (9) JM03-373PC2 (Rasmussen et al., 2007). (10) MSM5/5-712-2 (Müller et al., 2012; Werner et al., 2013; Aagaard-Sørensen et al., 2014). (11) NP05-71GC (Rasmussen et al., 2014). (12) JM10-330GC (Consolaro et al., 2018). (13) MSM5/5-723-2 (Müller et al., 2012; Werner et al., 2016). (14) NP05-11-70GC (Belt et al., 2015; Berben et al., 2017). (15) NP05-71GC (Klitgaard-Kristensen et al., 2013). (16) ASV880 (Duplessy et al., 2001). **(B)** Location of the investigated cores. The color of the star marking the location is defined by the dominant planktic foraminiferal species (dark blue: *N. pachyderma*; light blue: *T. quinqueloba*; red: *N. incompta*; black: *G. uvula*; light gray: other species) of each individual site during the different time intervals ($\mathbf{B_1}$: 12–11 ka BP. $\mathbf{B_2}$:11–10.2 ka BP. $\mathbf{B_3}$: 10.2–8.8 ka BP. $\mathbf{B_4}$: 8.8–7.4 ka BP. $\mathbf{B_5}$: 7.4–0 ka BP). The light blue stippled line indicates the location of the BSAF during the different time intervals represented by $\mathbf{(B_{1-5})}$. **(C)** Relative abundance of planktic foraminifera at the investigated sites over the last 12 ka BP. The color coding for the species is the same as in **(B)**. The stippled white lines indicate the transition phases between the time intervals of $\mathbf{(B_{1-5})}$. The white dots at the bottom of each panel indicate the tie-points for the age models that are within the 0–12 ka BP interval. Full information about all tie-points available is given in **Table 2**. Maps are created using GeoMapApp, http://geomapapp.org.

deglaciation. The relative distribution of the three species in a given core at a given time reflects on the water mass bathing the site. If a core was dominated by *N. incompta*, it was bathed by Atlantic Water. If the foraminiferal fauna was dominated by *N. pachyderma*, it was bathed by Arctic Water. However, if a site was dominated by *T. quinqueloba*, it was located close to the Arctic front. Depending on whether the second dominant species was *N. incompta* or *N. pachyderma*, the site was closer to the Atlantic or Arctic side of the front, respectively. This first order interpretation is somewhat complicated by the fact that *N.*

TABLE 1 | Names of cores sites, geographic locations, water depths, and references to the first publication of the synthesized data.

Core	Latitude	Longitude	Water depth (m)	Size fraction counted (μm)	References
JM09-KA11-GC	74°87′N	16°48′E	345	100–1,000	Berben et al., 2014
MD99-2304	77°37.26′N	09°56.90′E	2,300	≥100	Ebbesen et al., 2007
M23258	75°N	14°E	1,768	≥150	Sarnthein et al., 2003
PSh-5159N	71°21.65′N	22°38.81′E	418	100–500	Risebrobakken et al., 2010
T-88-2	71°59.29′N	14°21.52′E	1,500	≥100	Hald and Aspeli, 1997; Hald et al., 2007
T-79-51/2	69°18.00′N	16°23.00′E	505	≥125	Hald et al., 1996

The size fraction in which the planktic foraminifera were counted is indicated for each individual core.

pachyderma presently also dominates the planktic foraminiferal fauna in the Atlantic derived WSC, rather than *N. incompta*, due to the strong heat loss taking place before reaching these latitudes. Being aware of this complication, in combination with having full assemblage information in all cores throughout the Holocene, it is still possible to identify which water mass bathed the sites at which time. We acknowledge that if it had been possible to present foraminiferal deposition flux rates, absolute abundance data or δ^{13}C data from all cores, in addition to the relative abundance data, the base for our interpretations of the BSAF locations would have been stronger. Unfortunately, such information is not available.

Turborotalita quinqueloba is, however, a small species that is underrepresented with up to 20% when counts are done at ≥150 μm or ≥125 μm relative to counts done at ≥100 μm (Husum and Hald, 2012). It is therefore likely that the relative abundance of *T. quinqueloba* is somewhat underestimated in M23258 and T-79-51/2 at the times when *T. quinqueloba* shows an elevated relative abundance. The implications of this fact will be taken into account throughout the discussion.

RESULTS AND DISCUSSION

The relative abundances of planktic foraminifera from all six cores are presented in **Figure 2C** and **Table 3**. Based on **Figure 2C**, four steps have been identified when the dominant species changed in one or several of the cores. The assemblage composition between the steps will be presented and discussed, and a conclusion on the location of the BSAF will be made for each time interval (**Figures 2B$_{1-5}$,C** and **Table 3**). Following the presentation of results, and discussion of these, for the individual time intervals, the four-step development of the BSAF will be discussed in relation to upstream oceanographic changes that took place through the early Holocene.

Ca. 12 to 11 ka BP: The BSAF Was Located Along the Western Barents Sea Margin

Between ca. 12 and 11 ka BP, no data exists from PSh-5159N and MD99-2304. At all other sites the planktic foraminiferal assemblages were dominated by *N. pachyderma*, except in T-79-51/2 (**Figure 2C** and **Table 3**). In T-79-51/2, the first half of this time interval was also dominated by *N. pachyderma*, however, from ca. 11.5 ka BP the Atlantic Water species occupied ca. 50% of the assemblage (**Figure 2C**). Since T-79-51/2 was counted at ≥125 μm rather than ≥100 μm the relative abundance of *T. quinqueloba* might be underestimated. *Turborotalita quinqueloba* would, however, not be the dominant species even if the relative abundance is underestimated by up to 20% (Husum and Hald, 2012). Cores T-88-2 and M23258, located at greater depths along the western Barents Sea margin recorded more than 80% of *N. pachyderma* (**Figure 2C** and **Tables 1**, **3**). Even if the relative abundance of *T. quinqueloba* is underestimated in M23258, *N.* pachyderma would be the dominant species. In JM09-KA11-GC, located just north of Bear Island, *T. quinqueloba* and *N. incompta* were both present in significant amounts, with *T. quinqueloba* as the second dominant species (**Figure 2C** and **Table 3**). Despite a higher content of *T. quinqueloba* and *N. incompta* in JM09-KA11-GC the overall fauna is representative of Arctic Water (Johannessen et al., 1994; Husum and Hald, 2012).

Several sites from the Fram Strait and west Spitsbergen shelf were barren in planktic foraminifera at this time, argued to result from a dominance of Polar Water, with a strong meltwater influence indicated by a high content of ice rafted debris (Rasmussen et al., 2014; Werner et al., 2016; Consolaro et al., 2018; **Figure 2A**: 11, 12, and 13). Information about relevant oceanographic conditions of the northern Barents Sea is scarce for this time interval. To our knowledge, no planktic foraminiferal assemblage record exists, however, Lubinski et al. (2001) argued for inflow of cold subsurface water. Sea ice reconstructions from the northern Barents Sea do not reach as far back as 12 ka BP (Belt et al., 2015; Berben et al., 2017; **Figure 2A**: 14), hence, no inference can be made regarding the relation between the sea ice margin and the location of the BSAF.

Based on the combined evidence from planktic foraminiferal assemblage data from the region, we argue that the Barents Sea was to a large extent bathed by cold Arctic Water masses between ca. 12 and 11 ka BP (**Figure 2B$_1$**). The very southernmost shelf site did see traces of Atlantic Water, even though the overall assemblage was representative of colder water conditions than today. With Arctic Water conditions at most sites, the BSAF was located west of the westernmost sites, at the western Barents Sea margin. However, the Atlantic Water masses bathing T-79-51/2 suggests that the BSAF turned eastwards at the

TABLE 2 | Radiocarbon dates, ash horizons and calibrated ages used to create the age models.

Identification	Core	Sample depth (cm)	Dated material	^{14}C date	ΔR	Calibrated age range ±1σ	Rel. Prob.	Calendar age BP 1950 (med. prob.)	Tie point used	Reference for individual dates
Tra-1063	JM09-KA11-GC	4.5	Mollusc dextral part of Bathyarca glacialis	925 ± 30	71 ± 21	456–508	1	483	483	Rüther et al., 2012
Tra-1064	*JM09-KA11-GC*	*4.5*	*Mollusc dextral part of Bathyarca glacialis*	*900 ± 35*	*71 ± 21*	*434–498*	*1*	*465*	*Not used*	Rüther et al., 2012
Tra-1065	JM09-KA11-GC	16	Mollusc sinistral part of Bathyarca glacialis	1880 ± 35	71 ± 21	1,298–1,386	1	1,350	1,350	Rüther et al., 2012
Beta-324049	JM09-KA11-GC	27.5	Islandiella norcrossi/helenae	4820 ± 30	71 ± 21	4,904–5,047	1	4,989	4,989	Berben et al., 2014
Tra-1066	*JM09-KA11-GC*	*33*	*Mollusc dextral part of Astarte elliptica*	*1990 ± 35*	*71 ± 21*	*1,409–1,517*	*1*	*1,465*	*Not used*	Rüther et al., 2012
Beta-315192	JM09-KA11-GC	40	Islandiella norcrossi/helenae	5870 ± 30	71 ± 21	6,190–6,263	1	6,225	6,225	Berben et al., 2014
Beta-315193	JM09-KA11-GC	44.5	Islandiella norcrossi/helenae	6890 ± 40	71 ± 21	7,301–7,396	1	7,343	7,343	Berben et al., 2014
Tra-1067	JM09-KA11-GC	55	Mollusc dextral part of Astarte sulcate	7630 ± 45	71 ± 21	7,950–8,069	1	8,017	8,017	Rüther et al., 2012
Beta-315194	JM09-KA11-GC	80.5	Islandiella norcrossi/helenae	9140 ± 40	71 ± 21	9,688–9,868	1	9,776	9,776	Berben et al., 2014
Tra-1068	*JM09-KA11-GC*	*82.5*	*Mollusc paired shell of Astarte elliptica*	*8140 ± 50*	*71 ± 21*	*8,451–8,583*	*1*	*8,524*	*Not used*	Rüther et al., 2012
Tra-1069	*JM09-KA11-GC*	*82.5*	*Mollusc sinistral part of Nucluana minuta*	*8315 ± 50*	*71 ± 21*	*8,665–8,668 8,670–8,883*	*0.011 0.989*	*8,775*	*Not used*	Rüther et al., 2012
Beta-315195	*JM09-KA11-GC*	*111*	*Elphidium excavatum*	*10900 ± 50*	*71 ± 21*	*1,2212–1,2472*	*1*	*12,327*	*Not used*	Berben et al., 2014
Tra-1070	JM09-KA11-GC	134.5	Mollusc paired shell of Yoldiella intermedia	10705 ± 55	71 ± 21	11,833–12,075	1	11,965	11,965	Rüther et al., 2012
Tua-4421	MD99-2304	2.5	Planktic foraminifera	1020 ± 30	71 ± 21	507–566 579–593	0.865 0.135	548	548	Hald et al., 2004
Tua-3911	MD99-2304	28.5	Planktic foraminifera	8295 ± 55	71 ± 21	8,628–8,847	1	8,745	8,745	Ebbesen et al., 2007
Tua-3913	MD99-2304	56.5	Planktic foraminifera	8450 ± 65	71 ± 21	8,858–9,075	1	8,964	8,964	Ebbesen et al., 2007
AA 36609	MD99-2304	80	Shell fragment	8965 ± 85	71 ± 21	9,461–9,656	1	9,564	9,564	Ebbesen et al., 2007
KIA9346	MD99-2304	130	Shell fragment	9670 ± 55	71 ± 21	10,397–10,562	1	10,475	10,475	Ebbesen et al., 2007
KIA9526	MD99-2304	156.5	Shell fragment	10030 ± 50	71 ± 21	10,836–11,044	1	10,935	10,935	Ebbesen et al., 2007
AA 36610	MD99-2304	186	Shell fragment	12170 ± 180	71 ± 21	13,374–13,747	1	13,568	13,568	Ebbesen et al., 2007
KIA9863	MD99-2304	215	Benthic foraminifera	12660 ± 70	71 ± 21	13,972–14,169	1	14,077	14,077	Ebbesen et al., 2007
KIA7648	M23258	25	*N. pachyderma*	1165 ± 35	71 ± 21	622–689	1	656	656	Sarnthein et al., 2003
KIA7649	M23258	51	*N. pachyderma*	2555 ± 30	71 ± 21	2,071–2,212	1	2,145	2,145	Sarnthein et al., 2003
KIA7650	M23258	67	*N. pachyderma*	3500 ± 35	71 ± 21	3,245–3,355	1	3,300	3,300	Sarnthein et al., 2003
KIA7651	M23258	93	*N. pachyderma*	4825 ± 40	71 ± 21	4,889–5,067	1	5,002	5,002	Sarnthein et al., 2003

(Continued)

TABLE 2 | Continued

Identification	Core	Sample depth (cm)	Dated material	^{14}C date	ΔR	Calibrated age range ±1σ	Rel. Prob.	Calendar age BP 1950 (med. prob.)	Tie point used	Reference for individual dates
KIA11534	M23258	118	*N. incompta*	6140 ± 70	71 ± 21	6,404–6,581	1	6,494	6,494	Sarnthein et al., 2003
KIA7653	M23258	154	*N. pachyderma*	7660 ± 45	71 ± 21	7,986–8,109	1	8,048	8,048	Sarnthein et al., 2003
KIA7654	M23258	177	*N. pachyderma*	8380 ± 45	71 ± 21	8,793–8,966	1	8,868	8,868	Sarnthein et al., 2003
KIA8553	M23258	192	*N. pachyderma*	8760 ± 40	71 ± 21	9,308–9,423	1	9,364	9,364	Sarnthein et al., 2003
KIA11535	M23258	207	*N. incompta*	8955 ± 55	71 ± 21	9,469–9,592	1	9,536	9,536	Sarnthein et al., 2003
KIA9193	M23258	241	*N. pachyderma*	9330 ± 70	71 ± 21	9,958–9,982 9,993–10,233	0.091 0.909	10,065	10,065	Sarnthein et al., 2003
KIA8554	*M23258*	*249*	*N. pachyderma*	*9235 ± 50*	*71 ± 21*	*9,868–10,090*	*1*	*9,955*	*Not used*	Sarnthein et al., 2003
KIA9354	M23258	250	*N. pachyderma*	9435≈55	71 ± 21	10,142–10,255	1	10,203	10,203	Sarnthein et al., 2003
KIA7657	M23258	315	*N. pachyderma*	10980 ± 70	71 ± 21	12,333–12,574 12,138–12,616	1	12,438	12,438	Sarnthein et al., 2003
KIA7658	M23258	355	*N. pachyderma*	12010 ± 55	71 ± 21	13,323–13,450	1	13,389	13,389	Sarnthein et al., 2003
KIA7659	M23258	394	*N. pachyderma*	12390 ± 60	71 ± 21	13,702–13,881	1	13,790	13,790	Sarnthein et al., 2003
Poz-15130	PSh-5159N	7.5	Mollusc fragments, benthic foraminifera	102.46_0.32 pMC	71 ± 21				Bomb carbon	Ivanova et al., 2003
Poz-20399	PSh-5159R	14.17	Lenticulina sp.	635 ± 30	71 ± 21	145–167 173–258	0.201 0.799	197	197	Ivanova et al., 2003
Poz-19995	PSh-5159N	21.5	Bulk foraminifera	1670 ± 30	71 ± 21	1,120–1,224	1	1,167	1,167	Ivanova et al., 2003
Poz-19997	PSh-5159N	40.5	Bulk foraminifera	2845 ± 30	71 ± 21	2,430–2,604	1	2,513	2,513	Risebrobakken et al., 2010
Poz-20568	PSh-5159N	45.5	Bulk foraminifera	4960 ± 40	71 ± 21	5,132–5,286	1	5,204	5,204	Risebrobakken et al., 2010
Poz-15131	PSh-5159N	50.5	Mollusc fragments	6105 ± 35	71 ± 21	6,392–6,499	1	6,450	6,450	Risebrobakken et al., 2010
Poz-19998	PSh-5159N	60.5	Bulk foraminifera	7040 ± 40	71 ± 21	7,423–7,506	1	7,471	7,471	Risebrobakken et al., 2010
Poz-12701	PSh-5159N	69.5	Brachiopod	7500 ± 40	71 ± 21	7,843–7,938	1	7,891	7,891	Risebrobakken et al., 2010
Poz-19999	PSh-5159N	86.5	Bulk foraminifera	8550 ± 50	71 ± 21	9,006–9,165	1	9,099	9,099	Risebrobakken et al., 2010
Poz-15132	PSh-5159N	99.5	Mollusc fragments, benthic foraminifera, ostracode	9700 ± 50	71 ± 21	10,435–10,586	1	10,515	10,515	Risebrobakken et al., 2010
Poz-19991	PSh-5159R	122.5	Mollusc	10010 ± 50	71 ± 21	10,804–11,013	1	10,908	10,908	Risebrobakken et al., 2010 Chistyakova et al., 2010
Poz-15133	PSh-5159N	133.5	Mollusc fragments	10290 ± 50	71 ± 21	11,150–11,259	1	11,209	11,209	Risebrobakken et al., 2010
Poz-12629	PSh-5159N	148.5	Astarte crenata	10360 ± 50	71 ± 21	11,193–11,349	1	11,284	11,284	Risebrobakken et al., 2010
Poz-16594	PSh-5159R	241	Bulk benthic foraminifera	12150 ± 70	71 ± 21	13,428–13,618	1	13,528	13,528	Risebrobakken et al., 2010 Chistyakova et al., 2010

(Continued)

TABLE 2 | Continued

Identification	Core	Sample depth (cm)	Dated material	^{14}C date	ΔR	Calibrated age range ±1σ	Rel. Prob.	Calendar age BP 1950 (med. prob.)	Tie point used	Reference for individual dates
Poz-19992	PSh-5159R	333	Bulk benthic foraminifera	13550 ± 70	71 ± 21	15,531–15,826	1	15,669	15,669	Risebrobakken et al., 2010 Chistyakova et al., 2010
Gif	T-88-2	12	Planktic foraminifera	2480 ± 90	71 ± 21	1,915–2,155	1	2,049	2,049	Hald and Aspeli, 1997
Tua-3914	T-88-2	26.5	Planktic foraminifera	4155 ± 60	71 ± 21	4,020–4,022 4,026–4,228	0.007 0.993	4,127	4,127	Hald and Aspeli, 1997
Tua-3915	T-88-2	53.5	Planktic foraminifera	6285 ± 75	71 ± 21	6,555–6,751	1	6,658	6,658	Hald and Aspeli, 1997
Gif	T-88-2	72	Planktic foraminifera	6880 ± 100	71 ± 21	7,239–7,421	1	7,328	7,328	Hald and Aspeli, 1997
Gif	T-88-2	136	Planktic foraminifera	9390 ± 110	71 ± 21	9,945–10,263	1	10,134	10,134	Hald and Aspeli, 1997
Tua-116	T-88-2	168.55	Planktic foraminifera	9905 ± 400	71 ± 21	10,204–11,255	1	10,794	10,204	Hald and Aspeli, 1997
Tua-465	T-88-2	196	Planktic foraminifera	9470 ± 105	71 ± 21	10,136–10,399	1	10,250	10,399	Hald and Aspeli, 1997
Gif	*T-88-2*	*210*	*Planktic foraminifera*	*8520 ± 120*	*71 ± 21*	*89,13–9,259*	*1*	*9,059*	*Not used*	Hald and Aspeli, 1997
Tua-464	T-88-2	261	Planktic foraminifera	10510 ± 115	71 ± 21	11,323–11,781	1	11,582	11,582	Hald and Aspeli, 1997
Vedde Ash	T-88-2	278.5	Tephra					12,171	12,171	Rasmussen et al., 2006
Tua 466	T-88-2	308	Planktic foraminifera	11475 ± 75	71 ± 21	12,757–12,959	1	12,869	12,869	Hald and Aspeli, 1997
TUa-1119	T-79-51/2	2	*Yoldiella* sp.	905 ± 65	71 ± 21	763–834 842–909	0.503 0.497	826	826	Hald et al., 1996
TUa-948	T-79-51/2	60	*Yoldiella* sp.	4195 ± 65	71 ± 21	4,628–4,762 4,707–4,839	0751 0.249	4,717	4,717	Hald et al., 1996
TUa-949	T-79-51/2	134	*Yoldiella* sp.	8570 ± 65	71 ± 21	9,485–9,563 9,572–9,584 9,465–9,593	0.894 0.075 0.032	9,542	9,542	Hald et al., 1996
TUa-950	T-79-51/2	148	*Yoldiella* sp.	9335 ± 100	71 ± 21	10,407–10,693	1	10,540	10,407	Hald et al., 1996
TUa-1705	T-79-51/2	178	*Yoldiella* sp.	9430 ± 65	71 ± 21	10,574–10,741	1	10,668	10,741	Hald et al., 1996
TUa-951	T-79-51/2	226	*Yoldiella* sp.	9995 ± 90	71 ± 21	11,274–11,621 11,679–11,689	0.976 0.024	11,508	11,508	Hald et al., 1996
TUa-952	T-79-51/2	252	*Yoldiella* lenticula	10405 ± 95	71 ± 21	12,107–12,423 12,496–12,516	0.953 0.047	12,276	12,276	Hald et al., 1996
TUa-1121	T-79-51/2	288	*Yoldiella* sp.	10560 ± 90	71 ± 21	12,418–12,645	1	12,513	12,513	Hald et al., 1996
NSRL-2057	T-79-51/2	318	*Nuculana* sp.	10620 ± 70	71 ± 21	12,547–12,678	1	12,599	12,599	Hald et al., 1996

For all cores the core top age was set to the year of coring. The age of the Vedde ash is taken from Rasmussen et al. (2006). ^{14}C AMS dates not used for the age calculations are shown in italic.

TABLE 3 | The relative abundances of planktic foraminiferal species present in the six investigated marine sediment cores are given as mean values for each time interval.

Core	Size fraction counted (μm)	Species	5 (0–7.4 ka BP)	4 (7.4–8.8 ka BP)	3 (8.8–10.2 ka BP)	2 (10.2–11 ka BP)	1 (11–12 ka BP)
JM09-KA11-GC	100–1000	*N. pachyderma*	23	23	36	54	48
		T. quinqueloba	62	64	45	30	32
		N. incompta	10	11	16	13	16
		G. uvula	2	0	1	0	0
		Other species	3	2	2	3	4
MD99-2304	≥100	*N. pachyderma*	93	68	27	71	
		T. quinqueloba	4	22	56	16	
		N. incompta	3	8	14	12	
		G. uvula	0	0	1	0	
		Other species	0	2	2	1	
M23258	≥150	*N. pachyderma*	89	84	40	66	82
		T. quinqueloba	6	9	42	20	10
		N. incompta	4	6	13	10	6
		G. uvula	0	0	0	0	0
		Other species	1	1	5	4	2
PSh-5159N	100–500	*N. pachyderma*	23	5	9	21	
		T. quinqueloba	42	88	84	65	
		N. incompta	16	4	5	11	
		G. uvula	16	1	1	0	
		Other species	3	2	1	3	
T-88-2	≥100	*N. pachyderma*	58	33	14	51	89
		T. quinqueloba	13	37	64	13	3
		N. incompta	24	22	16	32	7
		G. uvula	1	0	1	0	0
		Other species	4	8	5	4	1
T-79-51/2	≥125	*N. pachyderma*	15	21	20	26	31
		T. quinqueloba	18	28	28	26	23
		N. incompta	54	43	43	37	36
		G. uvula	2	1	1	1	0
		Other species	11	7	8	10	10

The latter are representative for each step in the development from deglaciation to the present Barents Sea Arctic front location as illustrated in ***Figures 2B*$_{1-5}$**.

northeastern margin of the Lofoten Basin, just north of T-79-51/2 (**Figure 2B$_1$**).

Ca. 11 to 10.2 ka BP: The BSAF Covered the Southwestern Barents Sea, but All Sites Along the Western Barents Sea Margin Where Still Dominated by Arctic Water

The main difference between the ca. 12 to 11 ka BP and the ca. 11 to 10.2 ka BP time interval is that the southwestern Barents Sea site PSh-5159N recorded a total dominance of *T. quinqueloba* (**Figure 2C** and **Table 3**). In T-88-2, west of PSh-5159N, the relative abundance of *N. pachyderma* is reduced with 38%, but the site was still dominated by this polar species. *Neogloboquadrina incompta* still dominated the planktic foraminiferal assemblage in T-79-51/2. Further north, *N. pachyderma* was the dominant species, however, somewhat more *T. quinqueloba* was present compared to the previous time interval, and it increased in relative abundance after ca. 10.5 ka BP, both in M23258 and MD99-2304. As for the ca. 12 to 11 ka BP interval, taking into account the potential underestimation of the relative abundance of *T. quinqueloba* would not change the dominant species at T-79-51/2 or at M23258. Hence, T-79-51/2 was bathed by Atlantic Water, Psh-5159N was close to the BSAF and all the other sites were bathed by Arctic Water between ca. 11 and 10.2 ka BP (**Figure 2B$_2$**).

The west Spitsbergen shelf was still barren in foraminifera, feeling the influence of icebergs and Polar surface Water, indicating rather cold conditions and a more extensive sea ice cover than at present until 9.6 ka BP (Rasmussen et al., 2014; **Figure 2A**: 11). Based on dinoflagellates, it was also argued that, just north of M23258, sea ice was present through parts of the year (Rigual-Hernández et al., 2017; **Figure 2A**: 8). A comparable increase in relative abundance of *T. quinqueloba* to the one seen in M23258 and in MD99-2304 from ca. 10.5 ka BP is also seen

further north in the Fram Strait (Aagaard-Sørensen et al., 2014; Werner et al., 2016; Consolaro et al., 2018; **Figure 2A**: 10, 12, and 13). The area around Kveithola, close to JM09-KA11-GC, did no longer record the direct influence of ice sheet disintegration but was still under the influence of deglaciation processes (Lantzsch et al., 2017). At the PSh-5159N core site, it has been argued that a warm, fresh summer mixed layer was replaced by sea ice during winter (Risebrobakken et al., 2010; **Figure 2A**: 2). Furthermore, it has previously been argued that the southwestern Barents Sea was in close proximity to the Arctic front at this time, with relative abundances of *T. quinqueloba* reaching up to 80% (Aagaard-Sørensen et al., 2010; Risebrobakken et al., 2010; **Figure 2A**: 2 and 7). Information is scarce regarding the conditions in the northern Barents Sea, but it is argued that cold conditions prevailed at least until 8–7 ka BP (Lubinski et al., 2001). Again, existing sea ice reconstructions from the northern Barents Sea do not reach as far back in time (Belt et al., 2015; Berben et al., 2017; **Figure 2A**: 14). The relation between the sea ice extent and the BSAF is therefore unknown for this time interval.

Based on the information gained from our synthesis, supported by the existing literature as reviewed above, we infer that the BSAF during this time interval also followed the western Barents Sea margin, however, it turned further eastwards into the southern Barents Sea, reaching PSh-5159N (**Figure 2B$_2$**).

Ca. 10.2 to 8.8 ka BP: The BSAF Was Located in the Vicinity of Most Sites

At ca. 10.2 ka BP, a significant and abrupt change which resulted in an overall dominance of the Arctic front indicator *T. quinqueloba* is observed in the planktic foraminiferal fauna at all sites except PSh-5159N and T-79-51/2 (**Figure 2C**). *Turborotalita quinqueloba* was already the dominant species in PSh-5159N whereas the Atlantic Water species *N. incompta* remained the most abundant in T-79-51/2 (**Figure 2C**). Even if the relative abundance of *T. quinqueloba* should be somewhat underestimated in T-79-51/2, the conclusion that T-79-51/2 was bathed by Atlantic Water (**Figure 2B$_3$**) would not change. This overall dominance of *T. quinqueloba* lasted until ca. 8.8 ka BP. In particular, MD99-2304, M23258 and T-88-2 recorded mean relative abundances of *T. quinqueloba* of 56, 42, and 64%, respectively (**Figure 2C**; **Table 3**). Since the planktic foraminiferal abundance in M23258 is counted at $\geq$150 μm instead of $\geq$100 μm, the relative contribution of *T. quinqueloba* is likely underestimated at this site compared to MD99-2304 and T-88-2 (Husum and Hald, 2012). In that case, *T. quinqueloba* would be more dominant than already indicated. In JM09-KA11-GC and PSh-5159N the increased abundances of *T. quinqueloba* were, relative to the previous time interval, more gradual, respectively from 30 to 45% and from 65 to 84% (**Figure 2C** and **Table 3**).

In the Fram Strait and west of Svalbard similarly high abundances of *T. quinqueloba* have been recorded for this time interval (Werner et al., 2013, 2016; Aagaard-Sørensen et al., 2014; Rasmussen et al., 2014; Consolaro et al., 2018; **Figure 2A**: 10, 11, 12, and 13). In these studies, it has been argued that the increased *T. quinqueloba* abundances were associated with enhanced influence of Atlantic Water and increased sea surface temperatures. The Polar front, and the highly productive surface waters associated with the front, moved northwards (Consolaro et al., 2018; **Figure 2A**: 12), and the increased absolute abundance of planktic foraminifera seen west of Svalbard reflected a change from Polar to Atlantic Water at ca. 9.6 ka BP (Rasmussen et al., 2014; **Figure 2A**: 11). Werner et al. (2016) observed a limited sea ice extent in the northern Fram Strait between 11 and 8.5 ka BP (**Figure 2A**: 13). In the northern Barents Sea, the reduced spring sea ice concentrations recorded between ca. 9.5 and 8.5 ka BP were associated with a, relative to historical times, retreated ice margin (Berben et al., 2017; **Figure 2A**: 14). The lack of a correspondence between the reduced spring sea ice extent and a shift in the BSAF seems to imply that the sea ice extent is no driver behind the location of the BSAF in this part of the Barents Sea at this time. Although *T. quinqueloba* remained the dominant species in the southwestern Barents Sea, the occurrence of *G. uvula* has been attributed to an enhanced influence of Coastal Water (Aagaard-Sørensen et al., 2010; **Figure 2A**: 7).

We argue that the pronounced and sharp increase in *T. quinqueloba* seen within the three northernmost investigated cores on the western Barents Sea margin (**Figure 2C**), and in other sites west of Svalbard and in the Fram Strait (Werner et al., 2013, 2016; Aagaard-Sørensen et al., 2014; Rasmussen et al., 2014; Consolaro et al., 2018; **Figure 2A**: 10, 11, 12, and 13), reflects a rather fast eastwards migration of the BSAF (**Figure 2B$_3$**). More specifically, the high mean abundances of *T. quinqueloba* imply that the core sites were actually at the true location of the BSAF (Johannessen et al., 1994; Husum and Hald, 2012). The subtler fauna changes seen in JM09-KA11-GC indicate that the BSAF was slowly moving toward the core site but had not reached it yet (**Figure 2B$_3$**). The high relative abundance of *T. quinqueloba* in both T-88-2 and PSh-5159N implies a location close to the BSAF for both sites, and more specifically a front location just above (**Figure 2B$_3$**).

Ca. 8.8 to 7.4 ka BP: The BSAF Migrated Eastwards Influenced by a Strong Topographic Steering

At ca. 8.8 ka BP, the foraminiferal assemblage in MD99-2304 and M23258 changed abruptly from a *T. quinqueloba* to a *N. pachyderma* dominance (**Figure 2C** and **Table 3**). Within these records, the mean values of the cold Polar Water species *N. pachyderma* reached 68 and 84% between ca. 8.8 and 7.4 ka BP, respectively (**Figure 2C** and **Table 3**). Even if the potential *T. quinqueloba* underestimation in M23258 is taken into account, the site would be totally dominated by *N. pachyderma*. A smaller, but still significant, decrease in the relative abundance of *T. quinqueloba* was recorded for T-88-2, from 64% to 37%, associated with a small increase in *N. incompta* and other Atlantic species and a significant increase in *N. pachyderma* (**Figure 2C** and **Table 3**). Contrary, in JM09-KA11-GC and PSh-5159N, the relative abundance of *T. quinqueloba* continued to increase (**Figure 2C**). In T-88-2, JM09-KA11-GC and PSh-5159N the Arctic front indicator *T. quinqueloba* was still the

dominant planktic foraminiferal species throughout this time interval (**Figure 2C** and **Table 3**).

A similar increased abundance of *N. pachyderma* was observed at ca. 8.8 ka BP in a record from the western Svalbard slope, located between the MD99-2304 and M23258 core locations (Rasmussen et al., 2007; **Figure 2A**: 9). However, farther north on the west Spitsbergen continental margin, the Arctic front indicator *T. quinqueloba* remained dominant until ca. 7 ka BP (Werner et al., 2016; Consolaro et al., 2018; **Figure 2A**: 12 and 13). The latter core sites are from locations closer to the continental margin and at more shallow water depths compared to the more southern located cores from the western Svalbard slope, respectively MD99-2304 and M23258 (**Figure 2A**). A PIP_{25} index record from the west Spitsbergen continental margin documented a reduced sea ice cover between ca. 8.5 and 7 ka BP (Müller et al., 2012; **Figure 2A**: 13). Reduced spring sea ice conditions were also recorded in the northern Barents Sea (Berben et al., 2017; **Figure 2A**: 14), even though the northward heat advection reached a minimum during this interval (Risebrobakken et al., 2011; Eldevik et al., 2014). Both northern latitude spring and summer insolation was, however, high (Laskar et al., 2004) and may have influenced the spring sea ice retreat. In the southwestern Barents Sea, the relative contribution of *T. quinqueloba* has been used as an argument for a continued influence of Arctic front conditions (Aagaard-Sørensen et al., 2010; Risebrobakken et al., 2010; **Figure 2A**: 2 and 7).

Based on the data presented in **Figure 2C**, combined with the existing literature, we argue that the BSAF migrated further eastwards into the Barents Sea from ca. 8.8 ka BP (**Figure 2B$_4$**). More specifically, the BSAF has moved over the two northernmost core sites at the western Barents Sea margin, reaching a position close to where it is located at present (**Figure 2B$_4$**). This could be seen as contradicted by the remaining high relative abundance of *T. quinqueloba* at the site located at the continental margin slightly further north, from where it is argued that the front was still located in the vicinity of the site (Consolaro et al., 2018; **Figure 2A**: 12). However, as the site discussed by Consolaro et al. (2018) is from a shallower location, this record rather confirms the strong topographic steering of the BSAF location. The increased dominance of *T. quinqueloba* in JM09-KA11-GC and the continuously high relative abundance of the same species in PSh-5159N strongly argues for the BSAF to be at, or at least very close to, these core locations ca. 8.8 to 7.4 ka BP (**Figure 2B$_4$**). The BSAF was, however, moving away from T-88-2, compared to the previous time interval, as shown by the decreased relative abundance of *T. quinqueloba* (**Figures 2B$_4$,C**). The increase in *N. pachyderma* contemporary with the decrease in *T. quinqueloba* is interpreted as an indication that T-88-2 transfers toward present conditions, with a rather high content of *N. pachyderma* due to the strong heat loss from the Atlantic Water before reaching the site. Overall, the observed changes in the planktic foraminiferal fauna reflects a continuous eastwards migration of the BSAF (**Figure 2B$_4$**). In the northwestern areas, the BSAF location was directed by the topography of the area, more specifically the western Barents Sea and BIT margins.

Ca. 7.4 to 0 ka BP: The BSAF Was Close to Its Present Location

Between ca. 7.4 ka BP and present day, *N. pachyderma* continued to dominate the foraminiferal assemblages in MD99-2304 and M23258 with mean relative abundances of 93 and 89%, respectively (**Figure 2C** and **Table 3**). *Neogloboquadrina pachyderma* was also the most abundant species in T-88-2, occupying 58% of the planktic foraminiferal fauna. A gradual increase in relative abundance of *N. incompta* took place in the more southern located core T-79-51/2. In JM09-KA11-GC the relative abundance of *T. quinqueloba* stayed high, at 62%. Although *T. quinqueloba* remained the dominant species in PSh-5159N, with a stable value around 42%, the relative abundance of the front indicator was significantly smaller than in JM09-KA11-GC as well as compared with the previous time (**Figure 2C** and **Table 3**) interval. More specifically for PSh-5159N, increased abundances of *N. incompta* and other species (19%), indicative of warmer Atlantic Water (Bé and Tolderlund, 1971; Johannessen et al., 1994), and *G. uvula* (3%) associated with Coastal Water (Husum and Hald, 2012) have been recorded (**Figure 2C** and **Table 3**). Underestimated relative abundance of *T. quinqueloba* would not change the dominant species, neither in M23258 nor in T-79-51/2. Common for all sites is that the planktic foraminiferal assemblages in general represent an equivalent of the late Holocene assemblage compositions at the sites (**Figure 2C**).

The dominance of *N. pachyderma* between ca. 7.4 ka BP and present day is also seen at other sites on the western Svalbard margin, as well as further northeast into the Fram Strait, indicating generally cold conditions throughout the last ca. 7 ka BP (Werner et al., 2013, 2016; Rasmussen et al., 2014; Consolaro et al., 2018; **Figure 2A**: 10, 11, 12 and 13). Increased IP_{25} concentrations after ca. 7 ka BP point to an expanded sea ice extent in the Fram Strait (Müller et al., 2012; **Figure 2A**: 13), corresponding to overall decreasing summer mixed layer temperatures in the Nordic Seas realm (Risebrobakken et al., 2011). Furthermore, for this time interval the overall cold conditions documented by planktic foraminifera at the western Svalbard and Barents Sea margin correspond to colder bottom water, or increased influence of Arctic Water indicators, as documented by benthic foraminifera from northern Svalbard and the northern Barents Sea (Duplessy et al., 2001; Slubowska et al., 2005; Klitgaard-Kristensen et al., 2013; **Figure 2A**: 15, 16, and 17). As compared to the previous time interval, the increased relative abundance of planktic Atlantic Water indicators seen in the southwestern Barents Sea sites, T-79-51/2, T-88-2 and PSh-5159N, as well as the decreased relative abundance of *N. pachyderma* seen at JM09-KA11-GC, correspond to a reduced sea ice extent in the western Barents Sea (Berben et al., 2014; **Figure 2A**: 5). The warming in the southwestern Barents Sea, combined with the cooling along the Svalbard margin and with the Arctic bottom Water in the northern Barents Sea, implies that a larger fraction of the NwAC entered the Barents Sea through the NCaC from ca 7.4 ka BP.

Based on the results summarized in **Figure 2C**, combined with the knowledge from previous studies, we argue that the BSAF was located close to its present position over the last ca. 7.4 ka BP (**Figure 2B$_5$**). The overall dominance of *N. pachyderma* along the

western Svalbard and Barents Sea margin, indicative of a stronger influence of cold Arctic Water masses (Bé and Tolderlund, 1971; Johannessen et al., 1994; Pflaumann et al., 2003; Husum and Hald, 2012), is here interpreted as evidence for the sites being located further away from the BSAF, under conditions comparable to present-day (**Figure 2B$_5$**). The increased relative abundances of *N. incompta* and other Atlantic species in T-79-51/2, T-88-2, and PSh-5159N indicate an increased influence of Atlantic Water into the southwestern Barents Sea (Bé and Tolderlund, 1971; Johannessen et al., 1994), and hence an eastward movement of the BSAF relative to the previous time interval (**Figures 2B$_{4-5}$**). This interpretation is in line with previous findings from individual studies from the area (Risebrobakken et al., 2010; Berben et al., 2014; **Figure 2A**: 2 and 5). The Arctic front indicator *T. quinqueloba* still dominated the fauna at PSh-5159N, however, the strongly reduced relative abundance relative to the preceding time interval supports that the BSAF moved away from the site (**Figures 2B$_{4-5}$**). The relative abundance of *T. quinqueloba* was significantly lower in PSh-5159N than in JM09-KA11-GC, a site that was located underneath the BSAF (**Figures 2B$_5$,C**), as it is also today. The overall similarity between the planktic foraminiferal fauna of today, or the late Holocene, and the general fauna composition in all sites over the last ca. 7.4 ka BP supports the interpretation of a BSAF close to its present-day location (**Figure 2B$_5$**), with a strong topographic steering in the west, and the eastern position more defined by variable inflow of Atlantic Water by the NCaC. Some variability did occur in the relative abundance data also over the last 7.4 ka BP, especially in T-88-2 and in PSh-5159N (**Figure 2C**). We argue that this variability is of a different character than seen before. The changes in T-88-2 are primarily driven by more or less *N. pachyderma* balanced by less or more *N. incompta*, hence, indicating variability driven by a stronger or weaker heat loss in the NwAC before reaching T-88-2. The continuous occurrence of *G. uvula* in PSh-5159N documents significantly different conditions at this site after 7.4 ka BP, suggesting that the fauna variability was related to changes at the interface between Coastal and Atlantic Water rather than Atlantic and Arctic Water (Husum and Hald, 2012). Hence, all results combined point to a northeastward shift of the BSAF at ca. 7.4 ka BP into the Barents Sea toward the present-day location (**Figure 2B$_5$**).

The Establishment of the BSAF in Context of Upstream Changes in Advection of Atlantic Water

Presently, the BSAF is well constrained by the topography of the western Barents Sea, following the northern margin of the BIT (Loeng, 1991; Parsons et al., 1996; Harris et al., 1998). In the eastern Barents Sea, the BSAF location is less stationary and dependent on the strength of the Atlantic Water inflow (Loeng, 1991; Parsons et al., 1996; Loeng and Drinkwater, 2007). The above discussion sets the development of the BSAF from the deglaciation through the early Holocene. Following the deglaciation, not only the Barents Sea oceanography, but also the upstream oceanography of the eastern Nordic Seas experienced significant changes (e.g., Risebrobakken et al., 2011; Eldevik et al., 2014). Since the present BSAF is in part tightly linked to upstream changes in the NwAC, the relation between upstream changes in the NwAC taking place as the BSAF established should be evaluated.

The northward heat advection in the NwAC reached a post glacial maximum ca. 10 ka BP due to a major reorganization of the Atlantic circulation through the deglaciation (Risebrobakken et al., 2011; Eldevik et al., 2014). A maximum heat advection at ca. 10 ka BP is supported by the Norwegian Sea planktic foraminiferal assemblage data shown by Zhuravleva et al. (2017). Strong heat loss did, however, take place before the NwAC reached the Barents Sea margin, and the Atlantic Water submerged further south than at present until ca. 9 ka BP (Risebrobakken et al., 2011). This southern submerging of the northward flowing Atlantic Water is reflected by enhanced abundance of Atlantic Water indicating benthic foraminifera in JM09-KA11-GC and PSh-5159N (Risebrobakken et al., 2010; Groot et al., 2014), when the planktic foraminiferal fauna shows that Arctic Water, or the BSAF, was located over the same sites at the same time (**Figures 2B$_{1-3}$**). The eastern Nordic Seas and the Barents Sea experienced significant melt water influence until ca. 9 ka BP, in association with the final deglaciation (Risebrobakken et al., 2010, 2011; Rasmussen et al., 2014), supporting the Arctic Water and BSAF conditions inferred from the synthesized relative abundance data.

The eastward movement of the BSAF, toward its present location at the northwestern Barents Sea and western Spitsbergen margins (**Figure 2B$_4$**), corresponds to the northward movement of the zone of submergence and the diminishing influence of melt water (Risebrobakken et al., 2011). The inflow of Atlantic Water to the Barents Sea was, however, smaller than at present until ca. 7.4 ka BP, also in line with the diminishing northward heat advection that followed the ca. 10 ka BP advection maximum and the gradual return to normal salinities (Risebrobakken et al., 2011; Eldevik et al., 2014).

From around ca. 7.4 ka BP, the BSAF has likely been located within the range of its present location in the eastern Barents Sea (**Figure 2B$_5$**), with the absolute location influenced by variable strength of the Atlantic Water inflow (Loeng, 1991; Parsons et al., 1996; Loeng and Drinkwater, 2007). Our results show that the investigated sites along the western Barents Sea margin and at the Barents Sea opening were bathed by Arctic Water following the deglaciation. A gradual transition took place when the BSAF moved eastward toward, and eventually over, the sites, before the present day oceanographic conditions settled (**Figures 2B$_{1-5}$**). This transformation of the Barents Sea, from an Arctic Water dominated basin to the present-day situation, with the southern Barents Sea being bathed by Atlantic Water, is consistent with the overall oceanographic changes that took place in the eastern Nordic Seas throughout the early Holocene.

CONCLUSION

The Barents Sea went through significant changes following the deglaciation of the last ice age, from when the area was covered by a grounded ice sheet, until the present oceanographic state of

this shallow epicontinental sea. The upper water column of the Barents Sea was fully occupied by Arctic Water masses until ca. 11 ka BP, with an exception at T-79-51/2 in the southwestern corner, where Atlantic Water was present. T-79-51/2 was constantly under Atlantic Water influence over the last ca. 11.8 ka BP. Between ca. 12 and 11 ka BP, the BSAF was located west of the western Barents Sea margin. From ca. 11 to 10.2 ka, the BSAF moved slightly further east along the margin, but was still located west of the sites. However, the BSAF turned further eastwards into the southwestern Barents Sea, with PSh-5159N feeling the influence of frontal conditions. Between ca. 10.2 and 8.8 ka BP all sites, with exception of T-79-51/2, were located underneath the BSAF. From ca. 8.8 ka BP, the BSAF settled close to its present position east of the northern Barents Sea and western Spitsbergen margin, and was located over JM09-KA11-GC at the northern margin of the BIT. In the southwestern Barents Sea, the BSAF moved eastwards from the previous location, slightly further away from T-88-2 but still being present over PSh-5159N. From ca. 7.4 ka BP, conditions of a similar character to the present are shown at all sites, and a modern BSAF location is inferred. The establishment of the BSAF as discussed above is in agreement with the main oceanographic changes seen in the eastern Nordic Seas throughout the early Holocene.

AUTHOR CONTRIBUTIONS

BR had the initial idea for the paper. BR and SB both contributed with data, to the discussions and to the writing of the paper.

ACKNOWLEDGMENTS

The research leading to this paper has received funding from the European Research Council under the European Research Council Framework Program (FP7/2007-2013) / ERC grant agreement n° 610055, building on work initiated through RCN projects 171159 (InAtc), ARCTREC, and POCAHONTAS. We thank Michael Sarnthein, Morten Hald, and Hanne Ebbesen for making published data available. Kira Rehfeld provided constructive suggestions on how to illustrate the results. We thank Anastasia Zhuravleva and Robert Spielhagen for their constructive feedback on the manuscript.

REFERENCES

Aagaard-Sørensen, S., Husum, K., Hald, M., and Knies, J. (2010). Paleoceanographic development in the SW Barents Sea during the Late Weichselian-Early Holocene transition. *Quat. Sci. Rev.* 29, 3442–3456. doi: 10.1016/j.quascirev.2010.08.014

Aagaard-Sørensen, S., Husum, K., Werner, K., Spielhagen, R. F., Hald, M., and Marchitto, T. M. (2014). A late glacial-early Holocene multiproxy record from the eastern Fram Strait, Polar North Atlantic. *Mar. Geol.* 355, 15–26. doi: 10.1016/j.margeo.2014.05.009

Bé, A. W. H., and Tolderlund, D. S. (1971). "Distribution and ecology of living planktonic foraminifera in surface waters of the Atlantic and Indian Oceans," in *The Micropalaeontology of the Oceans*, eds B. M. Funnell, and W. R. Riedel (Cambridge: Cambridge University Press), 105–149.

Belt, S. T., Cabedo-Sanz, P., Smik, L., Navarro-Rodriguez, A., Berben, S. M. P., Knies, J., et al. (2015). Identification of paleo Arctic winter sea ice limits and the marginal ice zone: optimised biomarker-based reconstructions of late Quaternary Arctic sea ice. *Earth Planet. Sci. Lett.* 431, 127–139. doi: 10.1016/j.epsl.2015.09.020

Berben, S. M. P., Husum, K., Cabado-Sanz, P., and Belt, S. T. (2014). Holocene sub-centennial evolution of Atlantic water inflow and sea ice distribution in the western Barents Sea. *Clim. Past.* 10, 181–198. doi: 10.5194/cp-10-181-2014

Berben, S. M. P., Husum, K., Navarro-Rodriguez, A., Belt, S. T., and Aagaard-Sørensen, S. (2017). Semi-quantitative reconstruction of early to late Holocene spring and summer sea ice conditions in the Northern Barents Sea. *J. Quat. Sci.* 32, 587–603. doi: 10.1002/jqs.2953

Blindheim, J., and Østerhus, S. (2005). "The Nordic Seas, main oceanographic features," in *The Nordic Seas: An integrated Perspective*, eds H. Drange, T. Dokken, T. Furevik, R. Gerdes, and W. Berger (Washington DC: American Geophysical Union), 11–38.

Carmack, E. C., Barber, D., Christensen, J. H., Macdonald, R., Rudels, B., and Sakshaug, E. (2006). Climate variability and physical forcing of the food webs and the carbon budget on panarctic shelves. *Prog. Oceanogr.* 71, 145–181. doi: 10.1016/j.pocean.2006.10.005

Chistyakova, N., Ivanova, E., Risebrobakken, B., Ovsepyan, E. A., and Ovsepyan, Y. S. (2010). Reconstruction of Postglacial environments in the southwestern Barents Sea based on foraminiferal assemblages. *Oceanology* 50, 573–581. doi: 10.1134/S0001437010040132

Consolaro, C., Rasmussen, T. L., and Panieri, G. (2018). Paleoceanographic and environmental changes in the eastern Fram Strait during the last 14,000 years based on benthic and planktonic foraminifera. *Mar. Micropaleontol.* 139, 84–101. doi: 10.1016/j.marmicro.2017.11.001

Duplessy, J.-C., Ivanova, E., Murdmaa, I., Paterne, M., and Labeyrie, L. (2001). Holocene paleoceanography of the northern Barents Sea and variations of the northward heat transport by the Atlantic Ocean. *Boreas* 30, 2–16. doi: 10.1080/030094801300062220

Ebbesen, H., Hald, M., and Eplet, T. H. (2007). Lateglacial and early Holocene climatic oscillations on the western Svalbard margin, European Arctic. *Quat. Sci. Rev.* 26, 1999–2011. doi: 10.1016/j.quascirev.2006.07.020

Eldevik, T., Risebrobakken, B., Bjune, A. E., Andersson, C., Birks, H. J. B., Dokken, T. M., et al. (2014). A brief history of climate - the northern seas from the Last Glacial Maximum to global warming. *Quat. Sci. Rev.* 106, 225–246. doi: 10.1016/j.quascirev.2014.06.028

Groot, D. E., Aagaard-Sørensen, S., and Husum, K. (2014). Reconstruction of Atlantic water variability during the Holocene in the western Barents Sea. *Clim. Past.* 10, 51–62. doi: 10.5194/cp-10-51-2014

Hald, M., Andersson, C., Ebbesen, H., Jansen, E., Klitgaard-Kristensen, D., Risebrobakken, B., et al. (2007). Variations in temperature and extent of Atlantic Water in the northern North Atlantic during the Holocene. *Quat. Sci. Rev.* 26, 3423–3440. doi: 10.1016/j.quascirev.2007.10.005

Hald, M., and Aspeli, R. (1997). Rapid climatic shifts of the northern Norwegian Sea during the last deglaciation and the Holocene. *Boreas* 26, 15–28. doi: 10.1111/j.1502-3885.1997.tb00648.x

Hald, M., Dokken, T., and Hagen, S. (1996). "Paleoceanography on the European arctic margin during the last deglaciation," in *Late Quaternary Paleoceanography of the North Atlantic Margins*, eds J. T. Andrews, W. E. N. Austin, H. Bergsten, and A. E. Jennings (London; Geological Society Special Publication), 275–287.

Hald, M., Ebbesen, H., Forwick, M., Godtliebsen, F., Khomenko, L., Korsun, S., et al. (2004). Holocene paleoceanography and glacial history of the west Spitsbergen area, Euro-Arctic margin. *Q. Sci. Rev.* 23, 2075–2088. doi: 10.1016/j.quascirev.2004.08.006

Harris, C. L., Plueddemann, A. J., and Gawarkiewicz, G. G. (1998). Water mass distribution and polar front structure in the western Barents Sea. *J. Geophys. Res.* 103, 2905–2917. doi: 10.1029/97JC02790

Hopkins, T. S. (1991). The GIN Sea: a synthesis of its physical oceanography and literature review, 1972–1985. *Earth Sci. Rev.* 30, 175–318. doi: 10.1016/0012-8252(91)90001-V

Hughes, A. L. C., Gyllencreutz, R., Lohne, Ø., Mangerud, J., and Svendsen, J. I. (2016). The last Eurasian ice sheets - a chronological database and time-slice reconstruction, DATED-1. Boreas 45, 1–45. doi: 10.101111/bor,112142

Husum, K., and Hald, M. (2012). Arctic planktic foraminiferal assemblages: implications for subsurface temperature reconstructions. *Mar. Micropaleontol.* 96–97, 38–47. doi: 10.1016/j.marmicro.2012.07.001

Ivanova, E. V., Ovsepyan, E. A., Risebrobakken, B., and Vetrov, A. A. (2003). Downcore distribution of living calcareous foraminifera and stable isotopes in the western Barents Sea. *J. Foraminiferal Res.* 38, 4, 337–356.

Johannessen, T., Jansen, E., Flatøy, A., and Ravelo, A. C. (1994). "The relationship between surface water masses, oceanographic fronts and paleoclimatic proxies in surface sediments of the Greenland, Iceland, Norwegian Seas," in *Carbon Cycling in Glacial Ocean: Constraints on the Ocean's Role in Global Change*, eds R. Zahn, M. Kominski, and L. Labyrie (New York, NY: Springer-Verlag), 61–85.

Klitgaard-Kristensen, D., Rasmussen, T. L., and Koc, N. (2013). Paleoceanographic changes in the northern Barents Sea during the last 16 000 years - new constraints on the last deglaciation of the Svalbard-Barents Sea Ice Sheet. *Boreas* 42, 798–813. doi: 10.1111/j.1502-3885.2012.00307.x

Kvingedal, B. (2005). "Sea-Ice Extent and Variability in the Nordic Seas, 1967–2002," in *The Nordic Seas: An Intergared Perspective*, Vol. 158, eds H. Drange, T. Dokken, T. Furevik, R. Gerdes, and W. Berger (Washington, DC: American Geophysical Union, Geophysical Monograph), 39–49.

Kwok, R. (2009). Outflow of Arctic Ocean Sea Ice into the Greenland and Barents Sea: 1979–2007. *J. Clim.* 22, 2438–2457. doi: 10.1175/2008JCLI2819.1

Kwok, R., Maslowski, W., and Laxon, S. W. (2005). On large outflows of Arctic sea ice into the Barents Sea. *Geophys. Res. Lett.* 32:L22503. doi: 10.21029/22005GL024485

Lantzsch, H., Hanebuth, T. J. J., Horry, J., Grave, M., Rebesco, M., and Schwenk, T. (2017). Deglacial to Holocene history of ice-sheet retreat and bottom current strength on the western Barents Sea shelf. *Quat. Sci. Rev.* 173, 40–57. doi: 10.1016/j.quascirev.2017.08.016

Laskar, J., Robutel, P., Joutel, F., Gastineau, M., Correia, A. C. M., and Levrard, B. (2004). A long-term numerical solution for the insolation quantities of the earth. *Astron. Astrophys.* 428, 261–285. doi: 10.1051/0004-6361:20041335

Loeng, H. (1991). Features of the physical oceanographic conditions of the Barents Sea. *Polar Res.* 10, 5–18. doi: 10.3402/polar.v10i1.6723

Loeng, H., and Drinkwater, K. (2007). An overview of the ecosystems of the Barents and Norwegian Seas and their response to climate variability. *Deep Sea Res. Part II* 54, 2478–2500. doi: 10.1016/j.dsr2.2007.08.013

Lubinski, D. J., Polyak, L., and Forman, S. L. (2001). Freshwater and Atlantic water inflow to the deep northern Barents and Kara seas since ca 13 ^{14}C ka: foraminifera and stable isotopes. *Quat. Sci. Rev.* 20, 1851–1879. doi: 10.1016/S0277-3791(01)00016-6

Mangerud, J., Bondevik, S., Gulliksen, S., Hufthammer, A. K., and Høisæter, T. (2006). Marine ^{14}C reservoir ages for 19th century whales and molluscs from the Northe Atlantic. *Quat. Sci. Rev.* 25, 3228–3245. doi: 10.1016/j.quascirev.2006.03.010

Müller, J., Werner, K., Stein, R., Fahl, K., Moros, M., and Jansen, E. (2012). Holocene cooling culminates in sea ice oscillations in Fram Strait. *Quat. Sci. Rev.* 47, 1–14. doi: 10.1016/j.quascirev.2012.04.024

Parsons, A. R., Bourke, R. H., Muench, R. D., Chiu, C.-S., Lynch, J. F., Miller, J. H., et al. (1996). The Barents Sea Polar Front in summer. *J. Geophys. Res.* 101, 14201–114221. doi: 10.1029/96JC00119

Pfirman, S. L., Bauch, D., and Gammelsrød, T. (1994). "The Northern Barents Sea: Water Mass Distribution and Modification," in *The Polar Oceans and Their Role in Shaping the Global Environment: The Nansen Centennial Volume*, eds O. M. Johannessen, R. D. Muench, and J. E. Overland (Washington DC: American Geophysical Union), 77–94.

Pflaumann, U., Sarnthein, M., Chapman, M., d'Abreu, L., Funnell, B. M., Huels, M., et al. (2003). Glacial North Atlantic Sea-surface conditions reconstructed by GLAMAP 2000. *Paleoceanography* 18:1065. doi: 10.1029/2002PA000774

Rasmussen, S. O., Andersen, K. K., Svensson, A. M., Steffensen, J. P., Vinther, B. M., Clausen, H. B., et al. (2006). A new Greenland ice core chronology for the last glacial termination. *J. Geophys. Res.* 111:D06102. doi: 10.01029/02005JD006079

Rasmussen, T. L., Thomsen, E., Skirbekk, K., Slubowska-Woldengen, M., Klitgaard-Kristensen, D., and Koc, N. (2014). Spatial and temporal distribution of Holocene temperature maxima in the northern Nordic seas: interplay of Atlantic-, Arctic- and polar water masses. *Quat. Sci. Rev.* 92, 280–291. doi: 10.1016/j.quascirev.2013.10.034

Rasmussen, T. L., Thomsen, E., Slubowska, M. A., Jessen, S., Solheim, A., and Koc, N. (2007). Paleoceanographic evolution of the SW Svalbard margin (76°N) since 20,000 14C yr BP. *Quat. Res.* 67, 100–114. doi: 10.1016/j.yqres.2006.07.002

Reimer, P. J., Bard, E., Bayliss, A., Beck, C. W., Blackwell, P. G., Bronk Ramsey, C., et al. (2013). IntCal13 and MARINE13 radiocarbon age calibration curves 0-50000 years cal BP. *Radiocarbon* 55, 1869–1887. doi: 10.2458/azu_js_rc.55.16947

Rigual-Hernández, A. S., Colmenero-Hidalgo, E., Martrat, B., Bárcena, M. A., de Vernal, A., Sierro, F. J., et al. (2017). Svalbard ice-sheet decay after the Last Glacial Maximum: new insights from micropalaeontological and organic biomarker paleoceanographic reconstructions. *Paleogeogr. Paleoclimatol. Paleoecol.* 465, 225–236. doi: 10.1016/j.palaeo.2016.10.034

Risebrobakken, B., Dokken, T., Smedsrud, L. H., Andersson, C., Jansen, E., Moros, M., et al. (2011). Early Holocene temperature variability in the Nordic Seas: the role of oceanic heat advection versus changes in orbital forcing. *Paleoceanography* 26:PA4206. doi: 10.1029/2011PA2117

Risebrobakken, B., Moros, M., Ivanova, E., Chistyakova, N., and Rosenberg, R. (2010). Climate and oceanographic variability in the SW Barents Sea during the Holocene. *Holocene* 20, 609–621. doi: 10.1177/0959683609356586

Rudels, B., Korhonen, M., and Schauer, U. (2015). Circulation and transformation of Atlantic water in the Eurasian Basin and the contribution of the Fram Strait inflow branch to the Arctic Ocean heat budget. *Prog. Oceanogr.* 132, 128–152. doi: 10.1016/j.pocean.2014.04.003

Rüther, D. C., Bjarnadottir, L. R., Junttila, J., Husum, K., Rasmussen, T. L., Lucchi, R. G., et al. (2012). Pattern and timing of the northwestern Barents Sea Ice Sheet deglaciation and indications of episodic Holocene deposition. *Boreas* 41, 494–512. doi: 10.1111/j.1502-3885.2011.00244.x

Sarnthein, M., van Kreveld, S., Erlenkauser, H., Grootes, P. M., Kucera, M., Pflaumann, U., et al. (2003). Centennial-to-millennial-scale periodicities of Holocene climate and sediment injections off the western Barents shelf, 75°N. *Boreas* 32, 447–461. doi: 10.1080/03009480301813

Slubowska, M. A., Koç, N., Rasmussen, T. L., and Klitgaard-Kristensen, D. (2005). Changes in the flow of Atlantic water into the Arctic Ocean since the last deglaciation: evidence from the northern Svalbard continental margin, 80°N. *Paleoceanography* 20:PA4014. doi: 10.1029/2005PA001141

Smedsrud, L. H., Esau, I., Ingvaldsen, R. B., Eldevik, T., Haugan, P. M., Li, C., et al. (2013). The Role of the Barents Sea in the Arctic Climate System. *Rev Geophys.* 51, 415–449. doi: 10.1002/rog.20017

Sorteberg, A., and Kvingedal, B. (2006). Atmospheric Forcing on the Barents Sea Winter Ice Extent. *J. Clim.* 19, 4772–4784. doi: 10.1175/JCLI3885.1

Stuiver, M., and Reimer, P. J. (1993). Extended 14C database and revised CALIB radiocarbon calibration program. *Radiocarbon* 35, 215–230. doi: 10.1017/S0033822200013904

Vinje, T. (1977). Sea ice conditions in the European sector of the marginal seas of the Arctic, 1966–1975. *Årbok Norsk Polarinstitutt* 1975, 163–174.

Werner, K., Müller, J., Husum, K., Spielhagen, R. F., Kandiano, E. S., and Polyak, L. (2016). Holocene sea subsurface and surface water masses in the Fram Strait - Comparisons of temperature and sea-ice reconstructions. *Quat. Sci. Rev.* 147, 194–209. doi: 10.1016/j.quascirev.2015.09.007

Werner, K., Spielhagen, R. F., Bauch, D., Hass, H. C., and Kandiano, E. S. (2013). Atlantic Water advection versus sea-ice advances in the eastern Fram Strait during the last 9 ka: multiproxy evidence for a two-phase Holocene. *Paleoceanography* 28, 283–295. doi: 10.1002/palo.20028

Zhuravleva, A., Bauch, H. A., and Spielhagen, R. F. (2017). Atlantic water heat transfer through the Arctic Gateway (Fram Strait) during the Last Interglacial. *Global Planet. Change* 157, 232–243. doi: 10.1016/j.gloplacha.2017.09.005

Conflict of Interest Statement: The authors declare that the research was conducted in the absence of any commercial or financial relationships that could be construed as a potential conflict of interest.